Published for SISSA by Springer

Received: *March 14, 2023*
Revised: *October 29, 2023*
Accepted: *November 9, 2023*
Published: *November 28, 2023*

The dynamics of zero modes in lattice gauge theory — difference between SU(2) and SU(3) in 4D

Yuhma Asano[a,b] **and Jun Nishimura**[c,d]

[a] *Faculty of Pure and Applied Sciences, University of Tsukuba, 1-1-1 Tennodai, Tsukuba, Ibaraki 305-8571, Japan*
[b] *Tomonaga Center for the History of the Universe, University of Tsukuba, 1-1-1 Tennodai, Tsukuba, Ibaraki 305-8571, Japan*
[c] *Theory Center, Institute of Particle and Nuclear Studies, High Energy Accelerator Research Organization (KEK), 1-1 Oho, Tsukuba, Ibaraki 305-0801, Japan*
[d] *Graduate University for Advanced Studies (SOKENDAI), 1-1 Oho, Tsukuba, Ibaraki 305-0801, Japan*

E-mail: asano@het.ph.tsukuba.ac.jp, jnishi@post.kek.jp

Abstract: The dynamics of zero modes in gauge theory is highly nontrivial due to its nonperturbative nature even in the case where the other modes can be treated perturbatively. One of the related issues concerns the possible instability of the trivial vacuum $A_\mu(x) = 0$ due to the existence of nontrivial degenerate vacua known as "torons". Here we investigate this issue for the 4D SU(2) and SU(3) pure Yang-Mills theories on the lattice by explicit Monte Carlo calculation of the Wilson loops and the Polyakov line at large β. While we confirm the leading $1/\beta$ predictions obtained around the trivial vacuum in both SU(2) and SU(3) cases, we find that the subleading term vanishes only logarithmically in the SU(2) case unlike the power-law decay in the SU(3) case. In fact, the 4D SU(2) case is marginal according to the criterion by Coste et al. Here we show that the trivial vacuum dominates in this case due to large fluctuations of the zero modes around it, thereby providing a clear understanding of the observed behaviors.

Keywords: Lattice Quantum Field Theory, Other Lattice Field Theories, Lattice QCD, Field Theories in Lower Dimensions

ArXiv ePrint: 2303.01008

https://doi.org/10.1007/JHEP11(2023)204

JHEP11(2023)204

Contents

1 Introduction

Zero modes in gauge theory play an important role when one considers the theory in a small box with periodic boundary conditions. Their dynamics is highly nontrivial, however, due to its nonperturbative nature even in the case where the other modes can be treated perturbatively. The importance of zero modes can be most clearly seen by recalling the large-N reduced model [1], which implies that the zero-mode effective theory can be actually equivalent to the original gauge theory under certain conditions [2, 3]. Furthermore, the maximally supersymmetric version of the large-N reduced model [4] is conjectured to be a nonperturbative formulation of superstring theory, in which (3+1)-dimensional expanding space-time is expected to emerge [5].

One of the issues related to the dynamics of zero modes in lattice gauge theory concerns the existence of nontrivial degenerate vacua known as "torons", which have constant diagonal link variables in each direction up to a gauge transformation. All these configurations minimize the plaquette action, which implies that they represent the orbit of vacua or the moduli space of the gauge field configurations. At weak coupling, the perturbative expansion can be performed by integrating out all the fluctuations including zero modes around each toron configuration, and one is left with the integration over the toron configurations. Then an important question is whether the trivial vacuum $U_{n,\mu} = \mathbf{1}$ dominates over the other toron configurations or not.

This question is answered in the affirmative for 4D SU(3) lattice gauge theory [6], and the leading $1/\beta$ correction to the Wilson loop have been obtained by perturbative

JHEP11(2023)204

expansion around the trivial vacuum. The 4D SU(2) case, on the other hand, turned out to be marginal according to the same criterion.

In this paper, we first show our Monte Carlo results for the Wilson loops at large β in the 4D SU(2) and SU(3) cases and compare them against the $O(1/\beta)$ predictions obtained by perturbation theory around the trivial vacuum. In the SU(3) case, our results approach the perturbative predictions as $\beta \to \infty$ with the deviation being suppressed by $\beta^{-1/2}$ compared to the leading $O(1/\beta)$ correction. In the SU(2) case, on the other hand, our results approach the perturbative predictions as well, but the approach turns out to be much slower than in the SU(3) case. The deviation is suppressed only by $O(1/\log\beta)$ compared to the leading $O(1/\beta)$ correction. This suggests that the trivial vacuum dominates as $\beta \to \infty$ in the SU(2) case as well although the fluctuations around it vanish much more slowly with increasing β than in the SU(3) case.

Here we attempt to understand this behavior of the 4D SU(2) lattice gauge theory by the effective theory for the zero modes around the trivial vacuum, which takes the form of the large-N reduced model at the leading order. In fact, it was noticed in section 3.3 of ref. [6] that the partition function of the zero-mode effective theory has logarithmic divergence as $\beta \to \infty$ in the 4D SU(2) case.[1] This is actually due to the power-law tail (with the power of -1) of the eigenvalue distribution [9] in the reduced model, which was investigated in the context of matrix models for superstrings. We argue that this power-law tail is responsible for not only the dominance of the trivial vacuum as $\beta \to \infty$ but also the unusual finite β effects.

We also calculate the Polyakov line at large β in order to confirm our conclusion. In particular, we find that the distribution of the Polyakov line is peaked near unity in both SU(2) and SU(3) cases, but the difference is that the distribution in the SU(2) case has a long tail, which vanishes only very slowly at large β.

The rest of this paper is organized as follows. In section 2, we present our Monte Carlo results for the Wilson loops at large β, and compare them with perturbative predictions. In section 3, we review the effective theory for the zero modes, which explains our results in the SU(3) case. In section 4, we discuss how our results in the SU(2) case can be understood from the viewpoint of the zero-mode effective theory. In section 5, we show our results for the Polyakov line, which confirm our understanding. Section 6 is devoted to a summary and discussions. In appendix A, we discuss the volume dependence of our results. In appendix B, we provide some supplementary information on our analysis.

2 Wilson loops v.s. perturbative predictions

In this section, we present our Monte Carlo results for the Wilson loops and compare them with perturbative predictions at large β. Let us consider an SU(N) gauge theory on an

[1] In ref. [7], non-perturbative treatment of the zero modes has been discussed in the context of the gradient flow used in a running coupling constant scheme. In particular, the logarithmic behavior in the SU(2) case has been discussed by using a simple example [8], in which $1/\log\beta$ appears in the perturbative expansion of the exact result.

JHEP11(2023)204

$L_1 \times \cdots \times L_D$ lattice with periodic boundary conditions with the action

$$S_{\rm g} = -\frac{\beta}{2N} \sum_n \sum_{\mu,\nu\neq\mu} {\rm tr}[U_{n,\mu} U_{n+\hat{\mu},\nu} U^\dagger_{n+\hat{\nu},\mu} U^\dagger_{n,\nu} - 1] \,, \tag{2.1}$$

where β is the inverse coupling constant squared. The Wilson loop of size $R_1 \times R_2$ is calculated by perturbation theory around the trivial vacuum $U_{n,\mu} = \mathbf{1}$ neglecting higher order terms than $\mathrm{O}(\beta^{-1})$ as [6]

$$W(R_1, R_2) = 1 - \frac{c_1^{(\rm tot)}}{\beta} + \mathrm{O}(\beta^{-\frac{3}{2}}) \,. \tag{2.2}$$

The coefficient $c_1^{(\rm tot)} = c_1^{(\rm zero)} + c_1^{(\rm nonzero)}$ consists of the zero-mode contribution

$$c_1^{(\rm zero)} = \frac{N^2-1}{2(D-1)V} (R_1 R_2)^2 \tag{2.3}$$

and the non-zero-mode contribution

$$c_1^{(\rm nonzero)} = \frac{N^2-1}{8V} \sum_{k\neq 0} \frac{1}{\sum_\mu \sin^2 \frac{k_\mu}{2}} \left(\left| e^{ik_1 R_1} - 1 \right|^2 \left| \sum_{m=0}^{R_2-1} e^{ik_2 m} \right|^2 + (1 \leftrightarrow 2) \right) , \tag{2.4}$$

where $k_\mu = \frac{2\pi}{L_\mu} n_\mu$ denotes the lattice momentum with n_μ being an integer. Note that the nonzero-mode contribution vanishes for a maximal Wilson loop with $R_1 = L_1$ and $R_2 = L_2$ since $e^{ik_1 R_1} = e^{ik_2 R_2} = 1$ in that case.

Let us first discuss the $N = 3$ case. In figure 1, we plot $\beta \left\{ 1 - W(R_1, R_2) \right\}$ for square Wilson loops ($R_1 = R_2$) on a 4^4 lattice with $\beta = 6 - 19200$.[2] While the 1×1 Wilson loop approaches $c_1^{(\rm tot)}$ monotonically, the larger Wilson loops show prominent overshooting behaviors. Moreover, the slope of the data points at the origin seems to be infinite for the latter case, which suggests that the subleading terms become non-analytic in $1/\beta$. In fact, we can fit $\beta \left\{ 1 - W(R_1, R_2) \right\}$ to $c_1^{(\rm tot)} + c\, \beta^{-1/2}$ as shown in figure 1 (Right) although for the 1×1 Wilson loop, the coefficient c is consistent with zero. Therefore, the Wilson loops for the SU(3) case are given by the expansion (2.2), where the subleading term is $\mathrm{O}(\beta^{-\frac{3}{2}})$. The coefficient of the non-analytic term $c\, \beta^{-1/2}$ increases with the size of the Wilson loop, which is responsible for the larger deviation from the leading perturbative prediction seen in figure 1 (Left). This is reasonable since the larger Wilson loops are more sensitive to quantum fluctuations in the infrared regime. The origin of this non-analytic term can be understood from the viewpoint of the zero-mode fluctuations [6] as we explain later.

Next we discuss the $N = 2$ case. In figure 2, we plot $\beta \left\{ 1 - W(R_1, R_2) \right\}$ for square Wilson loops ($R_1 = R_2$) on a 4^4 lattice with $\beta = 6 - 19200$. From figure 2 (Left) alone, it is not clear whether the data points are approaching $c_1^{(\rm tot)}$. However, figure 2 (Right) suggests

[2] Simulations at larger β require longer runs due to stronger auto-correlation. For instance, the auto-correlation time of the maximal Wilson loop at $\beta = 19200$ is estimated as 15000 trajectories for $N = 3$ and 50000 trajectories for $N = 2$. In order to get reasonable statistics, we have made 400000 trajectories for $N = 3$ and 1000000 trajectories for $N = 2$. See appendix B for the details.

JHEP11(2023)204

that $\beta\left\{1 - W(R_1, R_2)\right\}$ can be fitted to $c_1^{(\mathrm{tot})} + c/\ln\beta$ although for the 1×1 Wilson loop, the coefficient c is consistent with zero. In particular, this result shows that the trivial vacuum $U_{n,\mu} = \mathbf{1}$ dominates over the other toron configurations at large β even for the SU(2) case, which is not obvious from ref. [6]. We will provide clear understanding of this property as well as the appearance of the logarithmic term $c/\ln\beta$ from the viewpoint of the zero-mode effective theory.

3 Brief review of the zero-mode effective theory

In this section, we review the zero-mode effective theory following ref. [6]. We consider the classical solutions, which are given by toron configurations, and discuss the perturbative expansion around them including the zero modes. In particular, we find in the SU(3) case that the trivial vacuum dominates at large β and that the leading term in the Wilson loop can be obtained by using the zero-mode effective theory.

3.1 The effective action for the zero modes

The minima of the plaquette action are degenerate under periodic boundary conditions, and they are given, up to a gauge transformation, by torons $U^{(0)}_{n,\mu} = e^{iB_\mu}$, where B_μ is a constant real diagonal matrix. Let us expand the link variables around them as

$$U_{n,\mu} = e^{iQ_{n,\mu}}\, e^{iB_\mu}\,, \tag{3.1}$$

where $Q_{n,\mu}$ represents the fluctuations given by traceless Hermitian matrices satisfying

$$\frac{1}{V}\sum_n (Q_{n,\mu})_{ii} = 0 \qquad \text{for all } i\,. \tag{3.2}$$

Plugging (3.1) into (2.1), we obtain

$$S_{\mathrm{g}} = -\frac{\beta}{2N}\sum_n \sum_{\mu,\nu\neq\mu} \mathrm{tr}\left(e^{iQ_{n,\mu}} e^{i(1+D_\mu)Q_{n,\nu}} e^{-i(1+D_\nu)Q_{n,\mu}} e^{-iQ_{n,\nu}} - 1\right), \tag{3.3}$$

where $D_\mu Q_{n,\nu} = e^{i\,\mathrm{adj}(B_\mu)} Q_{n+\hat{\mu},\nu} - Q_{n,\nu}$ and $\mathrm{adj}(B_\mu) = [B_\mu,\ \cdot\ ]$.

Let us then decompose $Q_{n,\mu}$ as

$$Q_{n,\mu} = A_\mu + \tilde{A}_{n,\mu}\,, \tag{3.4}$$

where A_μ represents the zero modes, which satisfy $(A_\mu)_{ii} = 0$ for all i due to (3.2). The plaquette that appears in (3.3) can be expressed as

$$\begin{aligned}
&e^{iQ_{n,\mu}} e^{i(1+D_\mu)Q_{n,\nu}} e^{-i(1+D_\nu)Q_{n,\mu}} e^{-iQ_{n,\nu}} \\
&= \exp\Bigg[i\Big\{\Big(D_\mu\tilde{A}_{n,\nu} - D_\nu\tilde{A}_{n,\mu}\Big) + \Big(D_\mu A_\nu - D_\nu A_\mu\Big) + i\Big[A_\mu, A_\nu\Big] \\
&\qquad + i\left[A_\mu, D_\mu A_\nu - \frac{1}{2}D_\nu A_\mu\right] + i\left[D_\nu A_\mu - \frac{1}{2}D_\mu A_\nu, A_\nu\right] \\
&\qquad + \frac{i}{2}\Big[D_\nu A_\mu, D_\mu A_\nu\Big] + \cdots\Big\}\Bigg]\,,
\end{aligned} \tag{3.5}$$

JHEP11(2023)204

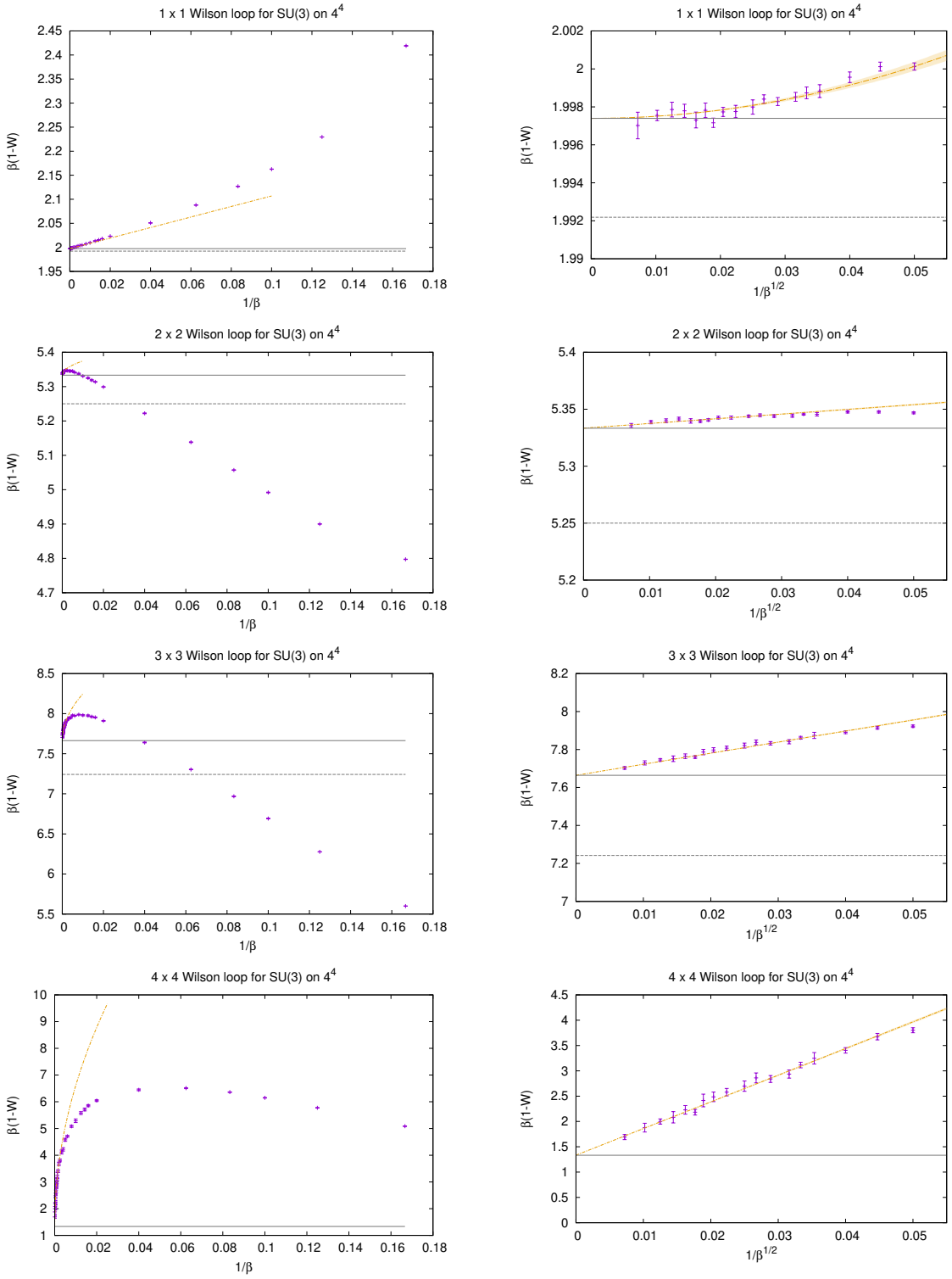

Figure 1. Monte Carlo results for $\beta\left\{1-W(R_1,R_2)\right\}$ on a 4^4 lattice are plotted against β (Left) and against $\beta^{-1/2}$ (Right) for $N=3$. The error bars are estimated by the jackknife method. The dashed and solid lines represent $c_1^{(\mathrm{nonzero})}$ and $c_1^{(\mathrm{tot})}$, respectively. Note that $c_1^{(\mathrm{nonzero})}=c_1^{(\mathrm{tot})}$ for the 4×4 maximal Wilson loop. The dash-dotted line represents a fit to the behavior $c_1^{(\mathrm{tot})}+c\,\beta^{-1/2}$ except for the 1×1 Wilson loop, which is fitted by $c_1^{(\mathrm{tot})}+c/\beta$.

JHEP11(2023)204

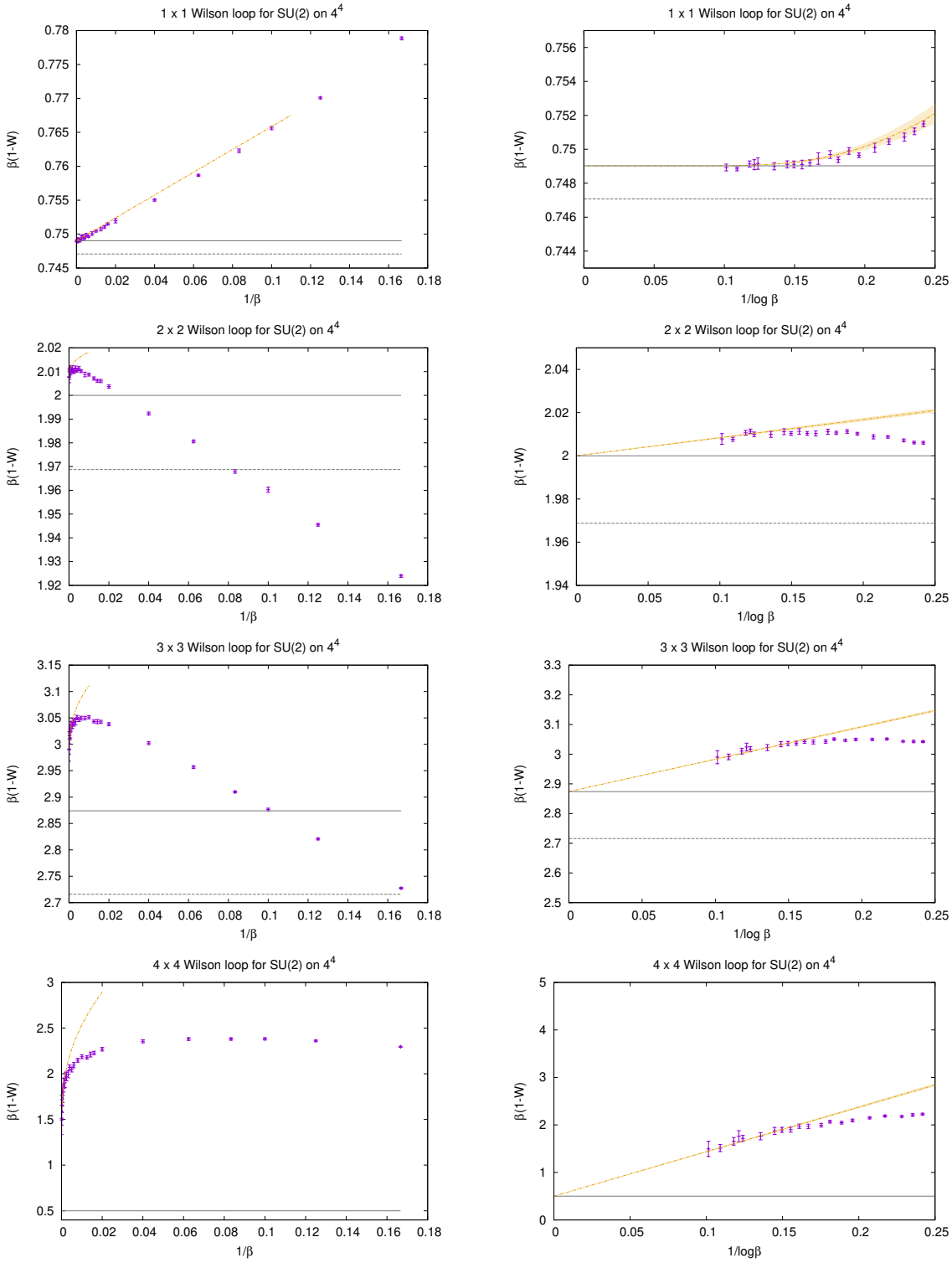

Figure 2. Monte Carlo results for $\beta\left\{1-W(R_1,R_2)\right\}$ on a 4^4 lattice are plotted against β (Left) and against $1/\log\beta$ (Right) for $N=2$. The error bars are estimated by the jackknife method. The dashed and solid lines represent $c_1^{(\mathrm{nonzero})}$ and $c_1^{(\mathrm{tot})}$, respectively. Note that $c_1^{(\mathrm{nonzero})}=c_1^{(\mathrm{tot})}$ for the 4×4 maximal Wilson loop. The dash-dotted line represents a fit to the behavior $c_1^{(\mathrm{tot})}+c/\log\beta$ except for the 1×1 Wilson loop, which is fitted by $c_1^{(\mathrm{tot})}+c/\beta$.

JHEP11(2023)204

where $D_\mu A_\nu = (e^{i\,\mathrm{adj}(B_\mu)} - 1)\,A_\nu$. Thus, the action can be rewritten as

$$S_{\mathrm{g}} = \frac{1}{2N} \sum_{\mu,\nu\neq\mu} \mathrm{tr} \left[\frac{\beta}{2} \sum_n \left(D_\mu \tilde{A}_{n,\nu} - D_\nu \tilde{A}_{n,\mu} \right)^2 - \beta V \left(U_\mu U_\nu U_\mu^\dagger U_\nu^\dagger - 1 \right) + \mathrm{O}\left((\beta V)^{-\frac{1}{4}} \right) \right], \tag{3.6}$$

where we have defined

$$U_\mu = e^{iA_\mu} e^{iB_\mu} \,. \tag{3.7}$$

From this, one finds that the elements of A_μ are generically of the order of $(\beta V)^{-\frac{1}{2}}$. Care should be taken when there exist i and $j \neq i$ such that $(B_\nu)_{ii} - (B_\nu)_{jj} = 0$ for any ν. In that case, one has $\left(\mathrm{adj}(B_\nu) A_\mu \right)_{ij} = 0$ for any ν. Therefore, one finds that the ij element of A_μ is of the order of $(\beta V)^{-\frac{1}{4}}$. Based on this power counting,[3] one finds that the terms abbreviated as $\cdots$ in (3.5) are of the order of $(\beta V)^{-\frac{1}{4}}$ at most. One can rewrite the Haar measure $dU_{n,\mu}$ in terms of dB_μ, dA_μ and $d\tilde{A}_{n,\mu}$ as

$$dU_{n,\mu} = dB_\mu \, dA_\mu d\tilde{A}_{n,\mu} \left(1 + \mathrm{O}(V^{\frac{1}{2}} \beta^{-\frac{1}{2}}) \right). \tag{3.8}$$

Let us introduce the gauge fixing term for the non-zero modes

$$S_{\mathrm{g.f.}} = \frac{\beta}{2N} \sum_n \mathrm{tr} \left[\left(\sum_\mu D_\mu \tilde{A}_{n,\mu} \right)^2 \right] = \frac{\beta}{2N} \sum_{k\neq 0} \mathrm{tr} \left| \sum_\mu (e^{i(k_\mu + \mathrm{adj}(B_\mu))} - 1) \tilde{A}_\mu(k) \right|^2 , \tag{3.9}$$

where $\tilde{A}_\mu(k)$ represents the Fourier modes of $\tilde{A}_{n,\mu}$. At the leading order in $1/\beta$, the partition function becomes

$$Z = \int dB_\mu \, dA_\mu d\tilde{A}_{n,\mu} \, dc \, d\bar{c} \, e^{-S_{\mathrm{zero}} - S_{\mathrm{nonzero}}} \,, \tag{3.10}$$

where c and $\bar{c}$ are the ghosts associated with the gauge fixing (3.9) and the actions for the zero modes and the nonzero modes are given, respectively, as

$$S_{\mathrm{zero}} = -\frac{\beta V}{2N} \sum_{\mu,\nu\neq\mu} \mathrm{tr} \left(U_\mu U_\nu U_\mu^\dagger U_\nu^\dagger - 1 \right), \tag{3.11}$$

$$S_{\mathrm{nonzero}} = \frac{\beta}{2N} \sum_{k\neq 0} \sum_{\mu,\lambda} 4 \,\mathrm{tr} \left\{ \tilde{A}_\mu(-k) \sin^2 \frac{k_\lambda + \mathrm{adj}(B_\lambda)}{2} \tilde{A}_\mu(k) + \bar{c}(-k) \sin^2 \frac{k_\lambda + \mathrm{adj}(B_\lambda)}{2} c(k) \right\} . \tag{3.12}$$

The expectation value of an observable $\mathcal{O}$ can be obtained as

$$\langle \mathcal{O} \rangle = \frac{1}{Z} \int dB_\mu \, dA_\mu d\tilde{A}_{n,\mu} \, dc \, d\bar{c} \, \mathcal{O} \, e^{-S_{\mathrm{zero}} - S_{\mathrm{nonzero}}} \,. \tag{3.13}$$

[3] Note that this power counting is not valid for the 4D SU(2) case, where the fluctuations in A_μ are larger than $\mathrm{O}((\beta V)^{-1/4})$.

JHEP11(2023)204

3.2 The integration over the torons

In this section, we discuss the integration over the torons B_μ, which represent the minimum action configurations.

As stated below (3.6), the order of magnitude of the zero modes A_μ depends on the toron configuration B_μ. Here we parametrize the toron configuration as

$$B_\mu^{(0)} = \begin{pmatrix} b_\mu^{(1)}\mathbf{1}_{V_1} & & & \\ & b_\mu^{(2)}\mathbf{1}_{V_2} & & \\ & & \ddots & \\ & & & b_\mu^{(M)}\mathbf{1}_{V_M} \end{pmatrix}, \tag{3.14}$$

where $(V_1, \cdots, V_M)$ is a partition of N, and consider the fluctuations $B_\mu = B_\mu^{(0)} + \tilde{B}_\mu$ around (3.14). The plaquette appearing in the action (3.11) for the zero modes can then be expanded as

$$\begin{aligned} &\sum_{\mu\neq\nu} \mathrm{tr}\left(e^{iQ_{n,\mu}} e^{i(1+D_\mu)Q_{n,\nu}} e^{-i(1+D_\nu)Q_{n,\mu}} e^{-iQ_{n,\nu}} - 1\right) \\ &= -\frac{1}{2}\,\mathrm{tr}\left[\left\{ i([B_\mu^{(0)}, A_\nu] - [B_\nu^{(0)}, A_\mu]) + i[\tilde{B}_\mu, A_\nu] - i[\tilde{B}_\nu, A_\mu] + i[A_\mu, A_\nu] \right.\right. \\ &\qquad - \left[A_\mu, [B_\mu^{(0)}, A_\nu] - \frac{1}{2}[B_\nu^{(0)}, A_\mu]\right] - \left[[B_\nu^{(0)}, A_\mu] - \frac{1}{2}[B_\mu^{(0)}, A_\nu], A_\nu\right] \\ &\qquad \left.\left. - \frac{i}{2}\left[[B_\nu^{(0)}, A_\mu], [B_\mu^{(0)}, A_\nu]\right]\right\}^2 + \cdots \right]. \end{aligned} \tag{3.15}$$

Thus, the elements of A_μ that appear in the action quadratically are those outside the $V_r \times V_r$ blocks. The number of such modes is

$$E_2(V) = (D-1)\left(N^2 - \sum_{r=1}^M V_r^2\right), \tag{3.16}$$

where -1 in the factor $(D-1)$ is due to the gauge fixing of the zero modes [6]. On the other hand, the elements of A_μ that appear quartically are those inside the $V_r \times V_r$ blocks. The number of such modes is

$$E_4(V) = D\sum_{r=1}^M (V_r^2 - 1), \tag{3.17}$$

after subtracting the number of modes corresponding to $B_\mu^{(0)}$. Each of the quadratic and quartic modes contribute to the partition function a factor of $O(\beta^{-1/2})$ and $O(\beta^{-1/4})$, respectively. Hence, the fluctuations around the toron labeled by $(V_1, \cdots, V_M)$ contribute to the partition function as

$$Z(V) \sim \beta^{-\{\frac{1}{2}E_2(V) + \frac{1}{4}E_4(V)\}}, \tag{3.18}$$

which implies that the toron configurations with V that minimizes $\frac{1}{2}E_2(V) + \frac{1}{4}E_4(V)$ give the dominant contribution. From this argument, one finds a critical dimension

$$D_c = \frac{2N}{N-1} \tag{3.19}$$

JHEP11(2023)204

such that for $D \leq D_c$, the dominant configuration corresponds to $M = N$ with $V_1 = V_2 = \cdots = V_N = 1$, while for $D \geq D_c$, it corresponds to $M = 1$ with $V_1 = N$.

In $D = 4$ dimensions, in particular, $N = 3$ corresponds to the latter case, which means that the trivial vacuum $B_\mu = 0$ dominates in the SU(3) case. On the other hand, $N = 2$ is marginal and one cannot determine the dominant toron configurations from this argument alone in the SU(2) case.[4]

3.3 Perturbative expansion of the Wilson loops

The discussion above implies that one can obtain the perturbative expansion of the Wilson loops for $N = 3$. Since the dominant toron is the trivial vacuum, B_μ fluctuates around 0; namely $B_\mu = \tilde{B}_\mu$. Expanding the zero-mode effective theory (3.11) with respect to A_μ and $\tilde{B}_\mu$ using (3.7), we obtain, at the leading order,

$$\begin{aligned} Z_0 &= \int dX_\mu \, e^{-S_0} \,, \\ S_0 &= -\frac{\beta V}{4N} \sum_{\mu \neq \nu} \mathrm{tr}[X_\mu, X_\nu]^2 \,, \end{aligned} \tag{3.20}$$

where $X_\mu = A_\mu + \tilde{B}_\mu$. Thus, the zero-mode contribution to the Wilson loop in (2.2) can be obtained by

$$-\frac{c_1^{(\mathrm{zero})}}{\beta} = \frac{1}{2N} (R_1 R_2)^2 \Big\langle \, \mathrm{tr} \left([X_1, X_2]^2 \right) \Big\rangle_0 \,, \tag{3.21}$$

where the expectation value $\langle \, \cdot \, \rangle_0$ is taken with respect to (3.20). Using the Schwinger-Dyson equation

$$-\frac{\beta V}{N} \sum_{\mu \neq \nu} \Big\langle \, \mathrm{tr}[X_\mu, X_\nu]^2 \Big\rangle = D \, (N^2 - 1) \,, \tag{3.22}$$

derived from (3.20), one obtains (2.3).

4 Understanding based on the reduced model

In this section, we show how the difference between SU(2) and SU(3) in 4D can be understood in terms of the zero-mode effective theory. For that, we have performed Hybrid Monte Carlo simulations of the zero-mode effective theory (3.20) for $N = 2$ and $N = 3$ with $D = 4$, where the coefficient βV in the action is set to unity since it can be absorbed by rescaling X_μ.

In figure 3 we plot the histogram of $\mathrm{tr}(\tilde{B}_\mu)^2$ for $N = 2$ and $N = 3$. We observe a peak near the origin for both cases, which suggests that the trivial vacuum dominates at large β not only for SU(3) but also for SU(2). However, the difference is that the histogram for the SU(2) case has a longer tail than that for the SU(3) case (Notice the scale of the horizontal axis.).

[4] According to this argument, nontrivial toron configurations dominate over the trivial vacuum at large β in the case of 3D SU(2) gauge theory and 2D SU(N) gauge theories with arbitrary N.

JHEP11(2023)204

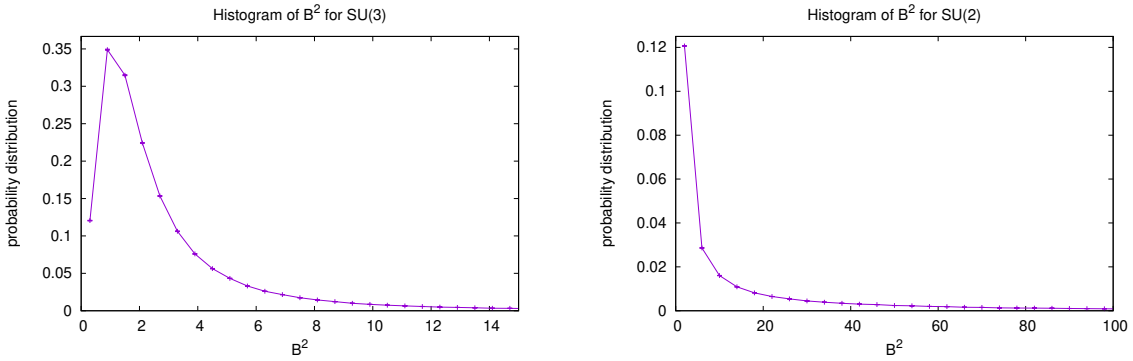

Figure 3. Histograms of $\frac{1}{N}\,\mathrm{tr}(B_\mu)^2$ obtained by simulating the zero-mode effective theory for $N = 3$ (Left) and $N = 2$ (Right).

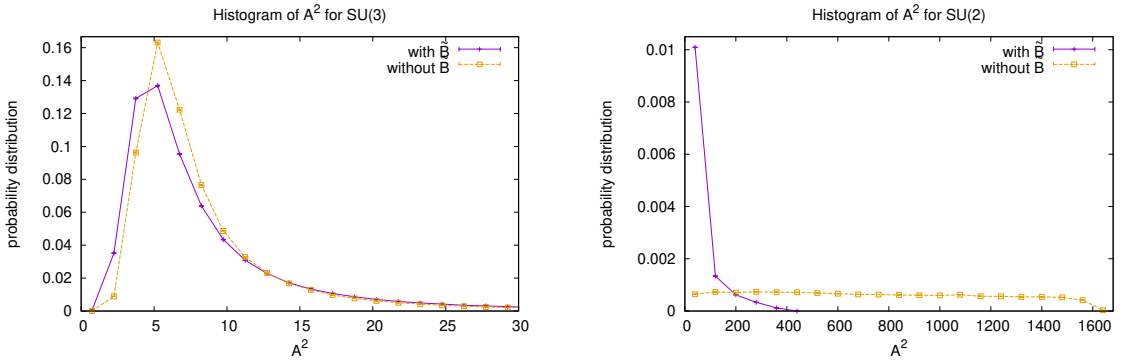

Figure 4. Histograms of $\frac{1}{N}\,\mathrm{tr}(A_\mu)^2$ obtained by simulating the zero-mode effective theory for $N = 3$ (Left) and $N = 2$ (Right). We also plot the results obtained by setting the fluctuations $\tilde{B}_\mu$ in the toron to zero for comparison.

In figure 4 we plot the histogram of $\mathrm{tr}(A_\mu)^2$ for $N = 2$ and $N = 3$, which shows that the results for $N = 2$ has a much longer tail than that for $N = 3$. In the same figure, we also plot the histogram obtained by setting $\tilde{B}_\mu$ in X_μ to zero, which corresponds to prohibiting the fluctuations in the toron. We observe that the histogram in the SU(2) case becomes almost flat with a sudden plunge at $\frac{1}{N}\,\mathrm{tr}(A_\mu)^2 \sim 1600$, which seems to indicate some problem in the simulation in this case. In any case, it is conceivable that the large fluctuations in the zero mode A_μ that appear around the trivial vacuum $\tilde{B}_\mu = 0$ are responsible for the dominance of the trivial vacuum $\tilde{B}_\mu = 0$.

The problem in the simulation for $N = 2$ can be seen also by checking the Schwinger-Dyson equation (3.22). In the case of setting $\tilde{B}_\mu = 0$, the right-hand side of eq. (3.22) should be replaced by $D(N^2 - N)$. In table 1 we show the left-hand side of the Schwinger-Dyson equation normalized by the constant on the right-hand side so that one obtains unity if the Schwinger-Dyson equation is satisfied. We find that the result is indeed unity within the error bar for $N = 3$, but not for $N = 2$. In figure 5 we plot the history of this quantity in the case without the fluctuations $\tilde{B}_\mu$ in the toron, which corresponds to the case with larger deviation from unity for the $N = 2$ case as one can see from table 1. We observe that

JHEP11(2023)204

	$N=3$	$N=2$
w/o $\tilde{B}_\mu$	0.999(3)	0.729(8)
w/ $\tilde{B}_\mu$	1.0009(12)	0.966(4)

Table 1. The expectation values of $-\frac{\beta V}{DN}\sum_{\mu\neq\nu}\langle \mathrm{tr}[X_\mu, X_\nu]^2\rangle$ normalized by N^2-1 or by N^2-N depending on whether $\tilde{B}_\mu$ is included or not.

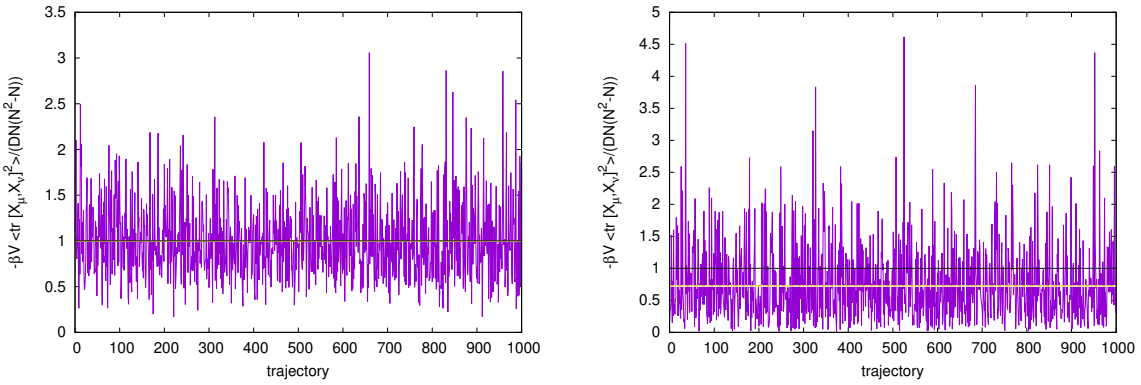

Figure 5. Histories of the quantity that is supposed to be unity theoretically due to the Schwinger-Dyson equation in the zero-mode effective theory for $N=3$ (Left) and $N=2$ (Right). The black horizontal line indicates the exact value, whereas the dashed line with a band indicates the measured expectation value with a statistical error. The two types of line coincide in the $N=3$ case.

the history for $N=2$ has larger spikes than that for $N=3$. From this observation with the fact that the expectation value is smaller than theoretically expected, it is conceivable that the simulation fails to sample rare configurations that give large spikes. We consider that this is due to the large fluctuations in A_μ that appear when the fluctuations $\tilde{B}_\mu$ in the toron become small.

These observations can be understood by recalling the dynamical properties of the reduced bosonic model (3.20). In particular, it was found that the eigenvalue distribution $\rho(x)$ of one of the D matrices, say X_1, in the model, has a power-law tail [9]

$$\rho(x) \sim x^{-p}\,, \qquad p = 2N(D-2) - 3D + 5 \tag{4.1}$$

except for $D=N=3$. Note that, in $D=4$, the power is $p=1$ for $N=2$ and $p=5$ for $N=3$. Since the partition function is given by $Z \sim \int_{-\infty}^{\infty} dx\, \rho(x)$, it converges for $N=3$, but diverges logarithmically[5] for $N=2$. When $B_\mu \neq 0$, one obtains quadratic terms in A_μ from (3.5), which suppress the fluctuations in A_μ. Therefore, in the $N=2$ case, the huge fluctuations in A_μ appear only when $B_\mu = 0$ and make $B_\mu = 0$ dominate at large β.

Next we discuss the slow convergence to the trivial vacuum, which is found to be described by the $1/\log\beta$ corrections in figure 2. Note first that, the fluctuations in A_μ is bounded by $\mathrm{O}(\beta^{-1/4})$ according to the effective theory (3.6) at large β even when $B_\mu = 0$. Therefore, the fluctuations in A_μ cannot be the reason for the slow convergence, and hence we focus on the fluctuations in B_μ, which will be denoted in what follows as B for simplicity.

[5]The logarithmic divergence of the partition function (3.20) for $N=2$ was found earlier in ref. [6] from a different argument. However, the dominance of the trivial vacuum was not concluded.

JHEP11(2023)204

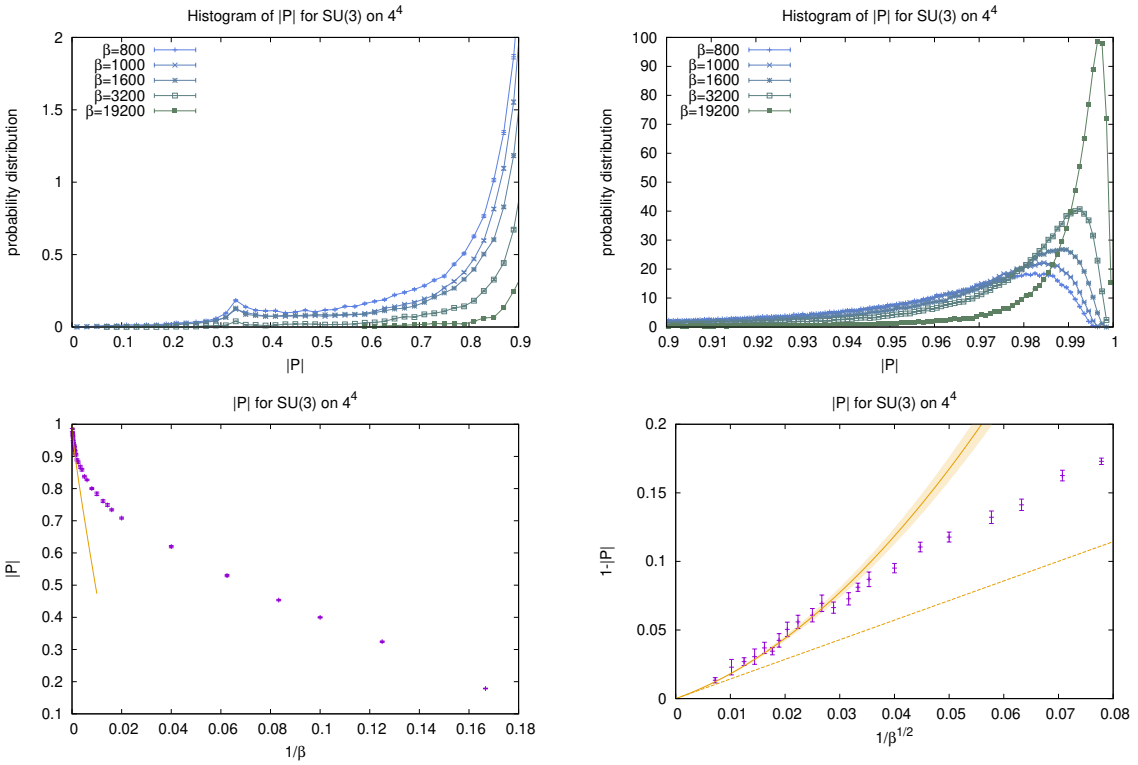

Figure 6. (Top) Histograms of $|P|$ for $N = 3$ on the 4^4 lattice. In the left panel, we show the region $0 \leq |P| \leq 0.9$ with the bin size 0.02, while in the right panel, we show the region $0.9 \leq |P| \leq 1$ with the bin size 0.001. (Bottom-Left) $|P|$ for $N = 3$ on the 4^4 lattice plotted against $1/\beta$. (Bottom-Right) $1 - |P|$ for $N = 3$ on the 4^4 lattice plotted against $1/\sqrt{\beta}$. The error bars in the bottom panels are estimated by the jackknife method. The dashed line represents the leading perturbative prediction (5.1). The solid line represents a fit assuming $\mathrm{O}(\beta^{-1})$ corrections.

Since the quadratic term in $(A_\mu)_{12}$ in the action has a coefficient $((B_\mu)_{11} - (B_\mu)_{22})^2 \sim B^2$, the partition function for B_μ after integrating out A_μ is suppressed at large B by $1/B^2$. At small B, on the other hand, the partition function for B_μ is expected to have a bound $\int dx\, \rho(x) \sim \ln \beta$ due to the power-law behavior (4.1) since β plays the role of a cutoff for the zero-mode effective theory. Combining these two asymptotic behaviors of the partition function for B_μ, the typical value of B can be roughly estimated by balancing $1/B^2$ and $\ln \beta$. This explains the slow convergence to the trivial vacuum.

5 Polyakov line v.s. perturbative predictions

In this section we provide further supports on our conclusion by measuring the Polyakov line for SU(2) and SU(3) on the 4^4 lattice with the same setup as in section 2. In particular, we show that the probability distribution of the Polyakov line exhibits a remarkable difference, which can be understood by the discussion in the previous section.

In figure 6, we present our results for SU(3) on the 4^4 lattice.[6] In the Top panels, we show the histogram of the Polyakov line $|P|$ for various β within the region $|P| \leq 0.9$ (Left)

[6]The auto-correlation time of the Polyakov line $|P|$ turned out to be almost the same as that of the maximal Wilson loop. See footnote 2 and appendix B for the details.

JHEP11(2023)204

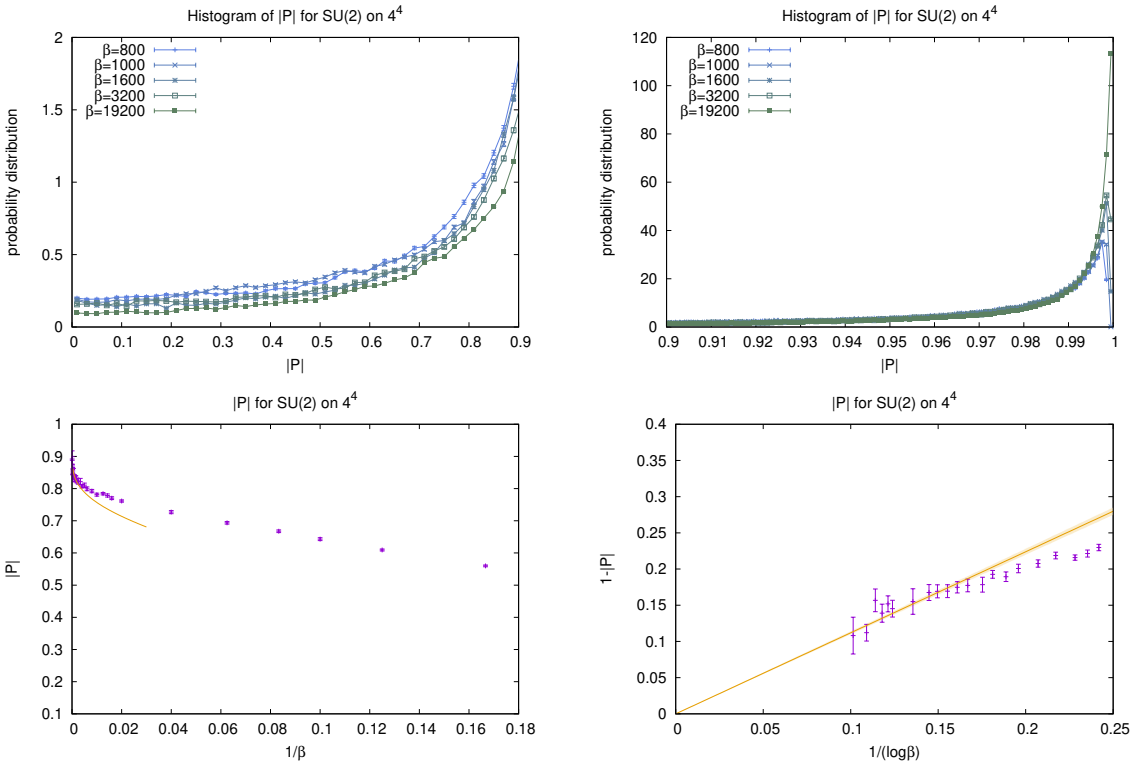

Figure 7. (Top) Histograms of $|P|$ for $N = 2$ on the 4^4 lattice. In the left panel, we show the region $0 \leq |P| \leq 0.9$ with the bin size 0.02, while in the right panel, we show the region $0.9 \leq |P| \leq 1$ with the bin size 0.001. (Bottom-Left) $|P|$ for $N = 2$ on the 4^4 lattice plotted against $1/\beta$. (Bottom-Right) $1 - |P|$ for $N = 2$ on the 4^4 lattice plotted against $1/\log\beta$. The error bars in the bottom panels are estimated by the jackknife method. The solid line represents a fit assuming $\mathrm{O}(1/\log\beta)$ corrections.

and $|P| \geq 0.9$ (Right), respectively. The peak near $|P| = 1$ becomes sharper and sharper for increasing β, which confirms that the trivial vacuum dominates and the zero-mode fluctuations are suppressed in the large β limit.

Using the perturbative expansion around $B_\mu = 0$, we obtain a prediction for the Polyakov line as

$$P = 1 - \frac{{L_4}^2}{2N}\left\langle \mathrm{tr}\left[(A_4 + \tilde{B}_4)^2\right]\right\rangle + \frac{{L_4}^4}{4!\,N}\left\langle \mathrm{tr}\left[(A_4 + \tilde{B}_4)^4\right]\right\rangle$$
$$- \frac{N^2-1}{2\beta V}\sum_{k\neq 0}\frac{1}{4\sum_\mu \sin^2\frac{k_\mu}{2}}\left|\sum_{m=0}^{L_4-1} e^{ik_4 m}\right|^2 + \mathrm{O}(\beta^{-\frac{3}{2}})\,. \tag{5.1}$$

The last term in the first line is logarithmically divergent for $N = 3$ due to the power-law tail (4.1). In the full lattice theory, this divergence is replaced by unpredictable $\mathrm{O}(\beta^{-1}\log\beta)$ terms, which are indistinguishable from the $\mathrm{O}(\beta^{-1})$ corrections. In the Bottom-Right panel, we plot $1 - |P|$ against $1/\sqrt{\beta}$ and compare our results against the $\mathrm{O}(\beta^{-1/2})$ perturbative prediction. We find that our results can be fitted by assuming $\mathrm{O}(\beta^{-1})$ corrections as expected from the above argument.

In figure 7, we show our results for the $N = 2$ case. From the Top panels, we find that the histogram of $|P|$ has a peak near $|P| = 1$, which becomes sharper and sharper for

JHEP11(2023)204

increasing β. However, the difference from the SU(3) case lies in the tail of the histogram, where the height of the histogram is decreasing but only slowly. From the Bottom-Left panel, it is not even clear whether the expectation value of $|P|$ is approaching unity as β increases. From the Bottom-Right panel, we find that $1 - |P|$ decreases as $1/\log\beta$ at large β, which is similar to the behavior of the Wilson loop in figure 2 (Right). These behaviors are consistent with our conclusion in section 4 that the trivial vacuum dominates at large β, while the fluctuations in the zero modes A_μ are large and decrease very slowly with increasing β.

6 Summary and discussions

In this paper we discussed a subtle issue in lattice perturbation theory for 4D SU(2) and SU(3) gauge theories with periodic boundary conditions. The minima of the action are actually degenerate and they are given by the toron configurations. For the SU(3) case, it is known that the trivial vacuum dominates over the nontrivial torons as $\beta \to \infty$, and the fluctuations of the zero modes are described by the effective theory, which takes the form of the bosonic reduced model. In the SU(2) case, the criterion on the dominance of the trivial vacuum discussed in the previous work is marginal. Our simulations on a 4^4 lattice have shown in this case that the Wilson loops at large β reproduce the leading $1/\beta$ correction obtained perturbatively around the trivial vacuum as shown in figure 2 although the subleading term decreases very slowly except for the 1×1 Wilson loop.

We have provided an explanation of this observation based on the zero-mode effective theory. Namely, the trivial vacuum dominates because the fluctuations in the zero modes become large around it as one can deduce from the power-law tail of the eigenvalue distribution in the reduced model. We have confirmed our conclusion by measuring the Polyakov line, which shows the dominance of the trivial vacuum as well as the large fluctuations in the zero modes at large β.

The issue addressed in this paper concerns any SU(N) gauge theory in a finite periodic box. Note, however, that it becomes irrelevant in the infinite-volume limit in which the boundary conditions have no effects. This can be understood since the gauge symmetry and the center symmetry allows us to restrict the integration domain of B_μ to [6][7]

$$-\frac{2\pi}{L_\mu} < (B_\mu)_{ii} - (B_\mu)_{jj} < \frac{2\pi}{L_\mu}\,, \tag{6.1}$$

which shrinks to zero in the $L_\mu \to \infty$ limit. On the other hand, the issue is relevant in a finite periodic box[8] *even in the continuum limit*, in which the toron configurations should

[7] In fact, one can use the center symmetry to restrict the integration domain of B_μ to

$$-\frac{N-1}{N}\frac{\pi}{L_\mu} < (B_\mu)_{ii} \le \frac{N-1}{N}\frac{\pi}{L_\mu}\,,$$

as one can prove explicitly for $N = 2$ and 3. However, this does not affect our discussion here.

[8] Such a set up is useful in making perturbative analyses applicable. For instance, QCD in a small box has been used recently in obtaining the critical point for color superconductivity based on the one-loop self-consistency equation [10].

JHEP11(2023)204

be described by $B_\mu^{\rm cont} \equiv B_\mu/a$, where a is the lattice spacing, since the integration domain of $B_\mu^{\rm cont}$ remains finite in the $L_\mu \to \infty$ limit with $L_\mu a$ fixed. In order to clarify these points, we have performed simulations on the 8^4 lattice and present our results for the Wilson loops and the Polyakov line in appendix A.

The subtlety in the 4D SU(2) gauge theory discussed in this paper is expected to be important also when one performs Monte Carlo simulations in a small box since the simulations may suffer from the ergodicity problem associated with the nontrivial dynamics of the zero modes. For instance, it was reported that the "two-color QCD" simulations on a $3^3 \times 64$ lattice with $N_{\rm f} = 2$ flavor Wilson quarks at finite density failed to reproduce the behavior of the quark number density expected for free quarks [11]. We suspect that there might be some problem in the simulations judging from the fact that our independent simulations with the same setup reproduce the expected behavior.

Finally let us recall that the trivial vacuum is expected *not* to dominate for the 3D SU(2) gauge theory according to the criterion of ref. [6] (See footnote 4.). Note, however, that the partition function of the naive zero-mode effective theory (3.20) diverges according to the eigenvalue distribution (4.1) for $D = 3$ and $N = 2$. This effect, which clearly favors the trivial vacuum, is not taken into account in the criterion of ref. [6]. Therefore we think it worth while to simulate this theory in a small box to see whether the prediction (2.2) around the trivial vacuum is approached or not in the large β limit.

Acknowledgments

We would like to thank Etsuko Itou for providing us with some results in 4D SU(2) gauge theory at finite density. We are also grateful to Yuta Ito, Hideo Matsufuru, Yusuke Namekawa, Asato Tsuchiya, Shoichiro Tsutsui and Takeru Yokota for discussions on finite density QCD, which motivated the present work. The computations were carried out on the PC clusters in KEK Computing Research Center and KEK Theory Center. We have used Bridge++ (http://bridge.kek.jp/Lattice-code/), which is a code set for numerical simulations of lattice gauge theories based on C++ [12, 13]. We would like to thank Hideo Matsufuru for his help concerning the usage of this code set.

JHEP11(2023)204

A Results on the 8^4 lattice

In this appendix, we present our result on the 8^4 lattice and discuss the behaviors of the Wilson loops and the Polyakov line at large β. In particular, we find that the effect of the zero modes is suppressed for small Wilson loops, whereas it remains to be important for large Wilson loops and the Polyakov line.

Let us first discuss the Wilson loops. In figures 8 and 9, we plot $\beta\left\{1-W(R_1,R_2)\right\}$ for square Wilson loops ($R_1 = R_2$) on the 8^4 lattice with $\beta = 3200-19200$ in the SU(3) case and the SU(2) case, respectively. In the SU(3) case, we find from figure 8 that $\beta\left\{1-W(R_1,R_2)\right\}$ can be fitted well with $c_1^{(\mathrm{tot})} + c\,\beta^{-1}$ except for the maximal 8×8 Wilson loop, which can be fitted to $c_1^{(\mathrm{tot})} + c\,\beta^{-1/2}$. Thus the $\mathrm{O}(\beta^{-1/2})$ contribution, which comes from the zero-mode fluctuations, is indeed suppressed for small Wilson loops on a larger lattice. In the SU(2) case, we find from figure 9 that the smaller (1×1 and 2×2) Wilson loops can be fitted by $c_1^{(\mathrm{tot})} + c\,\beta^{-1}$, whereas the larger ($4\times 4$ and 8×8) Wilson loops can be fitted by $c_1^{(\mathrm{tot})} + c/\ln\beta$. Thus the $\mathrm{O}(1/\ln\beta)$ contribution, which comes from the zero-mode fluctuations, is indeed suppressed for small Wilson loops on a larger lattice. Note also that the dominance of the trivial vacuum $U_{n,\mu} = \mathbf{1}$ holds in the SU(2) case as well as in the SU(3) case even on a larger lattice.

Let us next discuss the Polyakov line. In the Top panels of figure 10, we show our results for the SU(3) case. We find that the Polyakov line $|P|$ is consistent with the leading $\mathrm{O}(\beta^{-\frac{1}{2}})$ perturbative prediction in (5.1), where the coefficient is the same as in the case of the 4^4 lattice. We can also fit our data assuming subleading $\mathrm{O}(\beta^{-1})$ corrections. In the Bottom panels of figure 10, we show our results for the SU(2) case, where we find that $|P|$ can be fitted by assuming $\mathrm{O}(1/\ln\beta)$ corrections. Thus the Polyakov line exhibits the effect of the zero modes even on a larger lattice.

JHEP11(2023)204

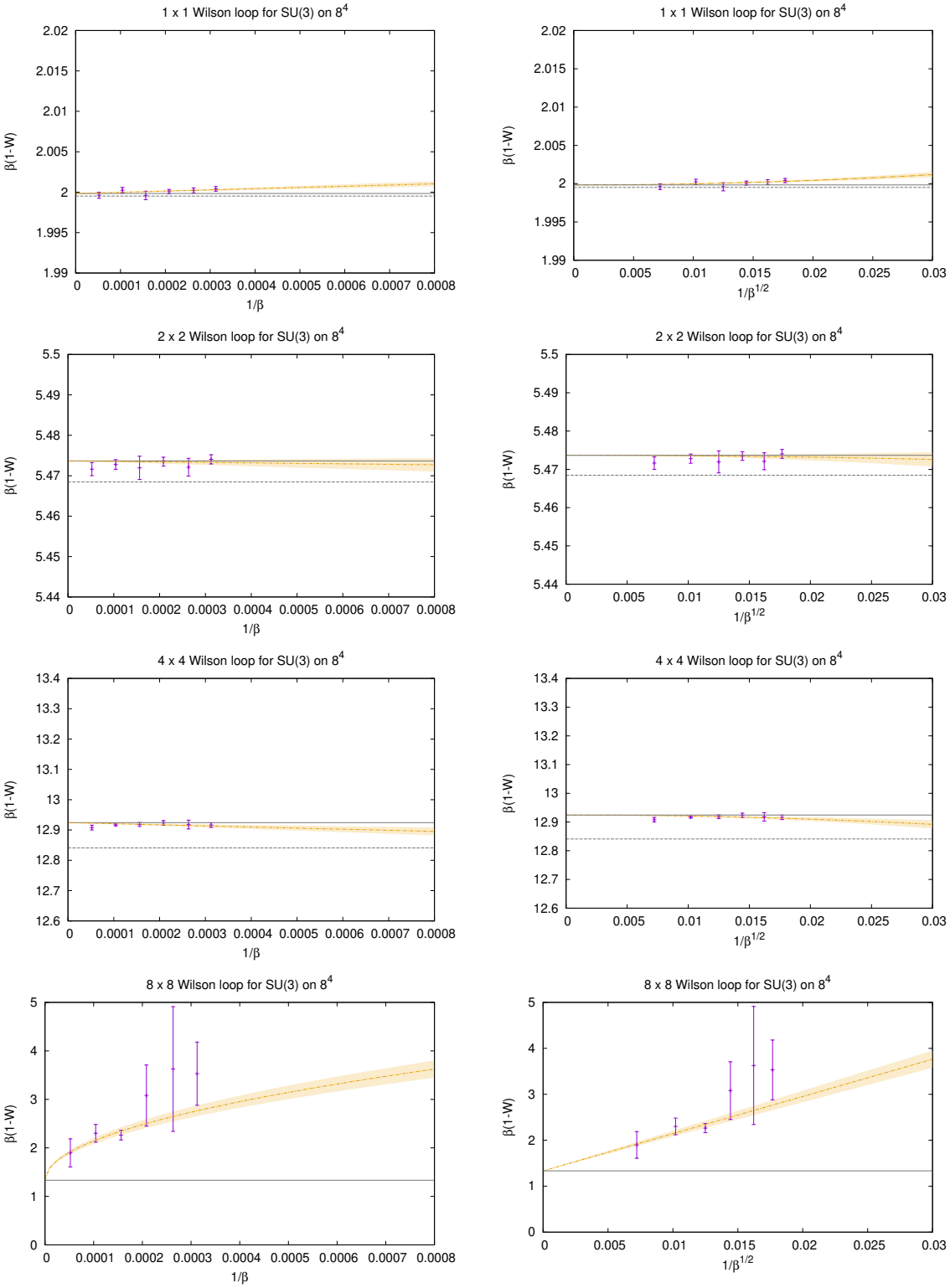

Figure 8. Monte Carlo results for $\beta\left\{1-W(R_1,R_2)\right\}$ on the 8^4 lattice are plotted against $1/\beta$ (Left) and against $\beta^{-1/2}$ (Right) for $N=3$. The error bars are estimated by the jackknife method. The dashed and solid lines represent $c_1^{(\mathrm{nonzero})}$ and $c_1^{(\mathrm{tot})}$, respectively. The dash-dotted line represents a fit to the behavior $c_1^{(\mathrm{tot})}+c/\beta$ for the 1×1, 2×2 and 4×4 Wilson loops and $c_1^{(\mathrm{tot})}+c\,\beta^{-1/2}$ for the 8×8 maximal Wilson loop.

JHEP11(2023)204

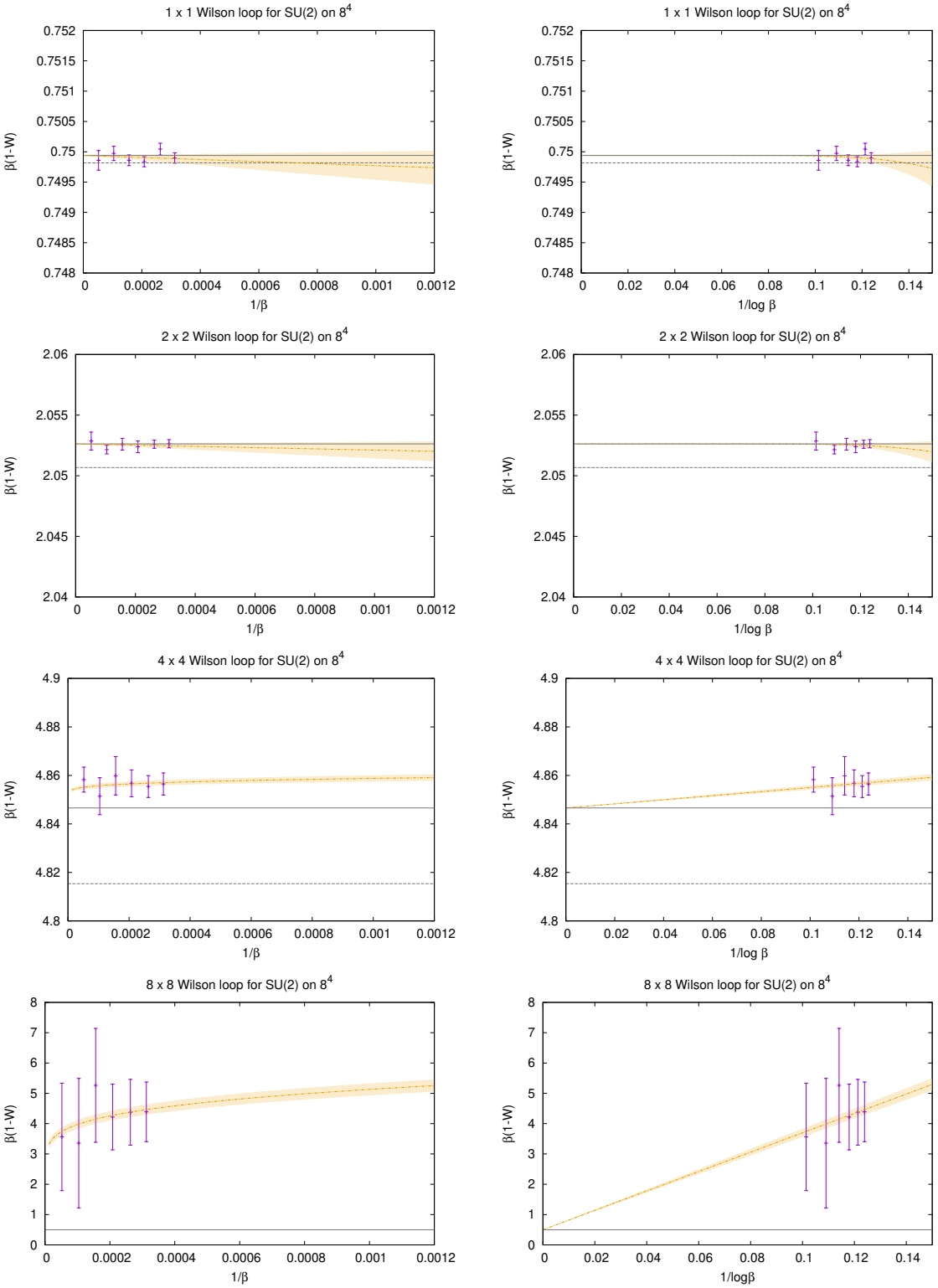

Figure 9. Monte Carlo results for $\beta\left\{1-W(R_1,R_2)\right\}$ on the 8^4 lattice are plotted against $1/\beta$ (Left) and against $1/\log\beta$ (Right) for $N=2$. The error bars are estimated by the jackknife method. The dashed and solid lines represent $c_1^{(\mathrm{nonzero})}$ and $c_1^{(\mathrm{tot})}$, respectively. The dash-dotted line represents a fit to the behavior $c_1^{(\mathrm{tot})}+c/\beta$ for the 1×1 and 2×2 Wilson loops, and $c_1^{(\mathrm{tot})}+c/\log\beta$ for the 4×4 and 8×8 Wilson loops.

JHEP11(2023)204

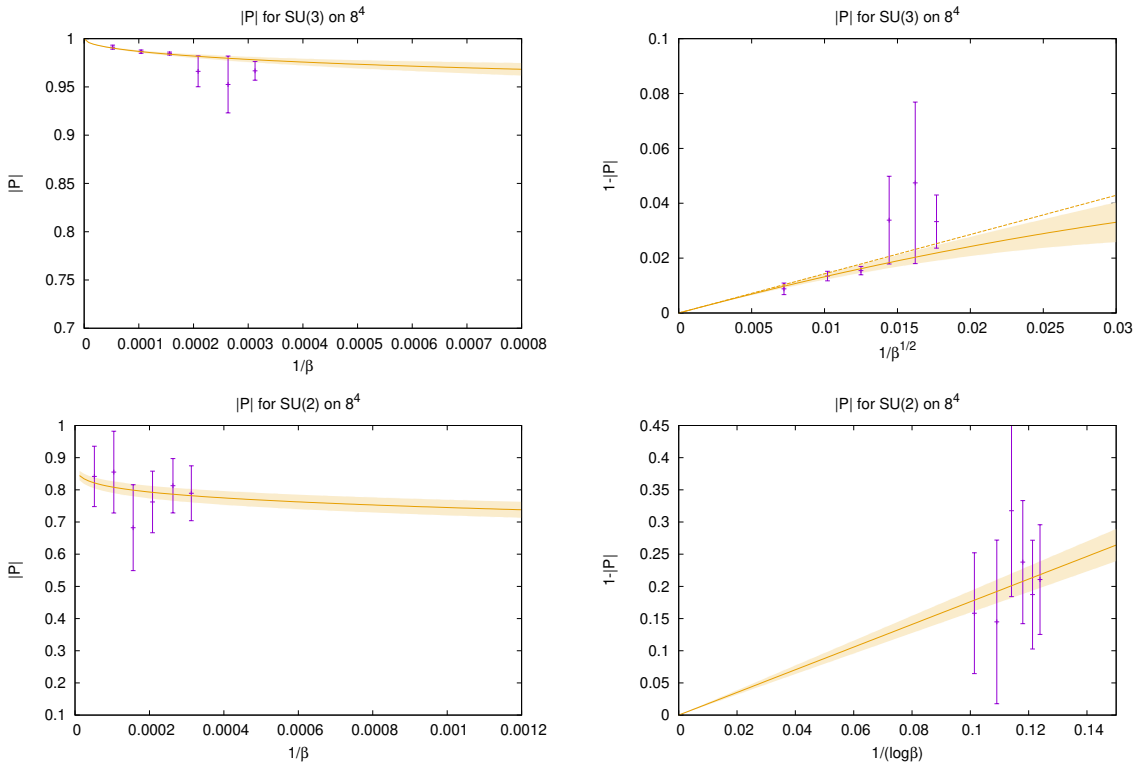

Figure 10. Monte Carlo results for the Polyakov line on the 8^4 lattice for $N = 2$ (Top) and 3 (Bottom). In the Left panels, $|P|$ is plotted against $1/\beta$, while in the Right panels, $1 - |P|$ is plotted against $1/\sqrt{\beta}$ for $N = 3$ and against $1/\log\beta$ for $N = 2$. The error bars are estimated by the jackknife method. The dashed line in the Top-Right panel for $N = 3$ represents the leading perturbative prediction (5.1). The solid line represents a fit assuming $\mathrm{O}(\beta^{-1})$ corrections for $N = 3$ and $\mathrm{O}(1/\log\beta)$ corrections for $N = 2$.

JHEP11(2023)204

B Supplementary information on our analysis

In this appendix, we provide some supplementary information on our analysis. The auto-correlation time of the quantities plotted in figures 1, 2, 6 and 7 are summarized in table 2 and 3. The information on the fitting shown in figures 1, 2, 6 and 7 are summarized in table 4 and 5.

			auto-correlation time				
$1/\beta^{\frac{1}{2}}$	β	trajectories	$W(1,1)$	$W(2,2)$	$W(3,3)$	$W(4,4)$	$\lvert P\rvert$
0.00722	19200	400000	5000	20000	5000	15000	15000
0.0102	9600	400000	1000	10000	1000	10000	10000
0.0204	2400	400000	5000	10000	4000	10000	10000
0.0289	1200	600000	2000	4000	2000	5000	6000
0.0400	625	400000	1000	2000	1000	3000	5000

Table 2. The total number of trajectories and the auto-correlation time in units of trajectories for the Wilson loops and the Polyakov line are presented in the SU(3) case.

			auto-correlation time				
$1/\log\beta$	β	trajectories	$W(1,1)$	$W(2,2)$	$W(3,3)$	$W(4,4)$	$\lvert P\rvert$
0.101	19200	1000000	4000	80000	5000	50000	50000
0.109	9600	1000000	15000	50000	20000	60000	60000
0.150	800	200000	1000	2000	1000	2000	4000
0.196	165	200000	500	10000	500	3000	40000
0.242	62.5	200000	1000	1000	2000	1000	10000
0.256	50	200000	10000	2000	10000	1000	2000

Table 3. The total number of trajectories and the auto-correlation time in units of trajectories for the Wilson loops and the Polyakov line are presented in the SU(2) case.

	$1/\sqrt{\beta}$	χ^2	d.o.f.	p-value
$W(1,1)$	0.00721–0.0354	10.4	14	0.73
$W(2,2)$	0.00721–0.0289	5.87	11	0.88
$W(3,3)$	0.00721–0.0448	12.2	16	0.73
$W(4,4)$	0.00721–0.0448	7.84	16	0.95
$\lvert P\rvert$	0.00721–0.0289	9.43	11	0.58

Table 4. The information on the fitting for the Wilson loops and the Polyakov line such as the fitting range, χ^2-value (before dividing by the degrees of freedom) and the p-value are presented in the SU(3) case.

JHEP11(2023)204

	$1/\log\beta$	χ^2	d.o.f.	p-value
$W(1,1)$	0.101–0.182	6.27	13	0.94
$W(2,2)$	0.101–0.145	10.0	7	0.19
$W(3,3)$	0.101–0.161	10.5	10	0.40
$W(4,4)$	0.101–0.161	7.67	10	0.66
$\lvert P\rvert$	0.101–0.167	9.19	11	0.60

Table 5. The information on the fitting for the Wilson loops and the Polyakov line such as the fitting range, χ^2-value (before dividing by the degrees of freedom) and the p-value are presented in the SU(2) case.

References

[1] T. Eguchi and H. Kawai, *Reduction of Dynamical Degrees of Freedom in the Large N Gauge Theory*, *Phys. Rev. Lett.* **48** (1982) 1063 [INSPIRE].

[2] A. Gonzalez-Arroyo and M. Okawa, *The Twisted Eguchi-Kawai Model: A Reduced Model for Large N Lattice Gauge Theory*, *Phys. Rev. D* **27** (1983) 2397 [INSPIRE].

[3] A. Gonzalez-Arroyo and M. Okawa, *Large N reduction with the Twisted Eguchi-Kawai model*, *JHEP* **07** (2010) 043 [arXiv:1005.1981] [INSPIRE].

[4] N. Ishibashi, H. Kawai, Y. Kitazawa and A. Tsuchiya, *A large N reduced model as superstring*, *Nucl. Phys. B* **498** (1997) 467 [hep-th/9612115] [INSPIRE].

[5] K.N. Anagnostopoulos et al., *Progress in the numerical studies of the type IIB matrix model*, arXiv:2210.17537 [DOI:10.1140/epjs/s11734-023-00849-x] [INSPIRE].

[6] A. Coste, A. Gonzalez-Arroyo, J. Jurkiewicz and C.P. Korthals Altes, *Zero Momentum Contribution to Wilson Loops in Periodic Boxes*, *Nucl. Phys. B* **262** (1985) 67 [INSPIRE].

[7] Z. Fodor et al., *The Yang-Mills gradient flow in finite volume*, *JHEP* **11** (2012) 007 [arXiv:1208.1051] [INSPIRE].

[8] Z. Fodor et al., *The gradient flow running coupling scheme*, *PoS* **LATTICE2012** (2012) 050 [arXiv:1211.3247] [INSPIRE].

[9] W. Krauth and M. Staudacher, *Eigenvalue distributions in Yang-Mills integrals*, *Phys. Lett. B* **453** (1999) 253 [hep-th/9902113] [INSPIRE].

[10] T. Yokota et al., *Color superconductivity on the lattice — analytic predictions from QCD in a small box*, *JHEP* **06** (2023) 061 [arXiv:2302.11273] [INSPIRE].

[11] S. Hands, T.J. Hollowood and J.C. Myers, *Numerical Study of the Two Color Attoworld*, *JHEP* **12** (2010) 057 [arXiv:1010.0790] [INSPIRE].

[12] S. Ueda et al., *Development of an object oriented lattice QCD code 'Bridge++'*, *J. Phys. Conf. Ser.* **523** (2014) 012046 [INSPIRE].

[13] Y. Akahoshi et al., *General purpose lattice QCD code set Bridge++ 2.0 for high performance computing*, *J. Phys. Conf. Ser.* **2207** (2022) 012053 [arXiv:2111.04457] [INSPIRE].

JHEP11(2023)204